Dalton Transactions

Phosphorus-based Ligand Effects on the Structure and Radical Scavenging Ability of Molecular Nanoparticles of CeO2

Journal:	*Dalton Transactions*
Manuscript ID	DT-ART-08-2021-002667.R1
Article Type:	Paper
Date Submitted by the Author:	26-Sep-2021
Complete List of Authors:	Christou, George; University of Florida, Department of Chemistry Russell-Webster, Bradley; University of Florida, Department of Chemistry Lopez-Nieto, Javi; University of Florida, Department of Chemistry Abboud, Khalil; University of Florida, Department of Chemistry

ARTICLE

Phosphorus-based Ligand Effects on the Structure and Radical Scavenging Ability of Molecular Nanoparticles of CeO_2

Received 00th January 20xx,
Accepted 00th January 20xx

DOI: 10.1039/x0xx00000x

Bradley Russell-Webster,[a,b] Javi Lopez-Nieto,[a] Khalil A. Abboud,[a] and George Christou [a]*

Two new Ce^{IV}/O^{2-} clusters, $(pyH)_8[Ce_{10}O_4(OH)_4(O_3PPh)_{12}(NO_3)_{12}]$ (**1**) and $[Ce_6O_4(OH)_4(O_2PPh_2)_4(O_2C^tBu)_8]$ (**2**), have been prepared that contain P-based ligands for the first time. They were obtained from the reaction of $(NH_4)_2[Ce(NO_3)_6]$, $PhPO_3H_2$ or Ph_2PO_2H, and $^tBuCO_2H$ in a 2:1:2 molar ratio in pyridine/MeOH (10:1 mL). Both compounds contain a $\{Ce_6O_4(OH)_4\}$ face-capped octahedral core, with **1** containing an additional four Ce^{IV} on the outside to give a supertetrahedral Ce_{10} topology; the $\{Ce_6O_8\}$ unit is the smallest reconizable fragment of the fluorite structure of CeO_2. The $HO^\bullet$ radical scavenging activities of **1** and **2** were measured by UV/vis spectral monitoring of methylene blue oxidation by $HO^\bullet$ radicals in the presence and absence of the Ce/O clusters, and the results compared with those for larger Ce_{24} and Ce_{38} molecular nanoparticles of CeO_2 prepared in previous work. **1** and **2** are both very poor $HO^\bullet$ radical scavengers compared with Ce_{24} and Ce_{38}, a result that is consistent with reports in the literature that PO_4^{3-} ions inhibit the radical scavenging ability of traditional CeO_2 nanoparticles and putatively assigned to PO_4^{3-} binding to the surface.

Introduction

Cerium dioxide (CeO_2) nanoparticles (CNPs, nanoceria) are widely used in catalysis, mechanical polishing, solid-oxide fuel cells, UV-shielding, and many other applications.[1–6] These take advantage of the ease with which Ce is able to cycle between the Ce^{3+} and Ce^{4+} states and the high surface area-to-volume ratio that nanosized materials exhibit. Both CNPs and ceria, the bulk parent material, possess the fluorite structure consisting of alternating layers of Ce^{4+} ions in eight-coordinate cubic geometry and O^{2-} ions in tetrahedral geometry. The fluorite lattice can readily accommodate the formation of O-vacancies with concomitant reduction of two Ce^{4+} ions, contributing to the reactivity of CNPs and ceria.

In the last 10-15 years, CNPs of size ≤20 nm have been of rapidly growing interest for biomedical applications owing to their impressive radical scavenging activity at ambient temperatures and the importance of minimizing damage to living tissue from such radicals, which contributes to several neuro0degenerative disorders.[7–11] In these applications CNPs have been identified as multi-functional. For example, they have the ability to operate as pro-oxidants or antioxidants, depending upon their physical properties such as Ce^{3+}/Ce^{4+} ratio, size and morphology, as well as their surface environments.[12–15]

The ability of CNPs to scavenge reactive oxygen species (ROS) such as $HO^\bullet$ radicals is related to the physiochemical properties of the material, particularly the ability to store and release O and the efficiency of the redox coupling between Ce^{3+} and Ce^{4+} ions.[16,17] Doping CNPs with redox-inactive Sm^{3+} to replace surface Ce^{3+} ions in the CNPs without altering the O-vacancy concentration resulted in a decrease in ROS scavenging ability compared with the non-doped CNPs, suggesting that Ce^{3+} ions are crucial for efficient ROS scavenging.[18] Similarly, it is assumed that as the CNP size decreases from 20 nm to 2 nm there is a concomitant increase in surface Ce^{3+} ions and O vacancies.[5] Hence, it is believed that smaller CNPs are likely better ROS scavengers, but multiple reports have also observed efficient radical scavenging by CNPs with low Ce^{3+} surface concentrations.[19] Such apparent conflicts in the CNP literature are likely due to the usual problem with traditional top-down nanoparticles, i.e., the range of sizes (polydispersity), shapes, and Ce^{3+}:Ce^{4+} ratios in CNP samples.

Some studies have demonstrated that environmental conditions can alter the ROS scavenging ability of CNPs. In the presence of H_2O_2, the superoxide dismutase (SOD) activity of CNPs is thought to be temporarily inhibited by the rapid oxidation of surface Ce^{3+} ions.[20a] Upon reduction of Ce^{4+} ions, the SOD activity increases, pointing to the importance of oxidation state changes for ROS scavenging ability. Of particular importance to the present work is the observation that CNPs are poor ROS scavengers in the presence of PO_4^{3-} ions, thought to be due to their binding to the surface and inhibiting somehow the ability to easily cycle between Ce^{3+} and Ce^{4+}.[20b–22]

We have recently demonstrated an alternative molecular bottom-up approach to ultra-small (<3 nm) CNPs by which they are synthesized as molecular clusters with the same fluorite structure as bulk CeO_2, and thus are what we now call

[a] *Department of Chemistry, University of Florida, Gainesville, FL 32611-7200, USA.*
[b] *Present address: Intel Corp., Hillsboro, OR.*
Electronic Supplementary Information (ESI) available: X-ray crystallographic data in CIF format, EPR spectra and packing diagrams. CCDC deposition codes 2100215 and 2100216 for **1** and **2**, respectively. For ESI and crystallographic data in CIF format, see DOI: 10.1039/x0xx00000x

'molecular nanoparticles' (MNPs). We have to date reported a family of ceria MNPs with Ce nuclearities up to Ce_{100} and Ce/O core dimensions up to ~2.4 nm.[23–25] They were prepared with a surface shell of carboxylate and pyridine ligands using mild solution reaction conditions at ambient temperatures. These MNP products bring to the field the benefits of molecular chemistry, particularly samples that are truly monodisperse (single-size), identical in shape, soluble, and crystalline, the latter allowing for complete characterization to atomic resolution by single-crystal X-ray crystallography.

One major advantage of the MNP approach is that their monodispersity allows reactivity properties to be determined as a function of exact size, shape and organic monolayer identity. The activity of the above MNPs as catalysts for ROS scavenging has been investigated for comparison with that of the larger CNPs.[24] Their hydroxyl radical ($HO^{\bullet}$) scavenging ability was monitored by EPR,[26] and it was found that it was size (nuclearity)-independent and decreased with increasing Ce^{3+}: Ce^{4+} ratio; this is contrary to many but not all the studies in the CNP literature, and this point is discussed in more detail elsewhere.[24] Notably, some of the Ce/O clusters assessed were able to completely scavenge all $HO^{\bullet}$ radicals prior to the first time point (one minute), indicating that these clusters have exceptional radical scavenging ability, better than the larger CNPs. It also shows that their ultra-small size of ≤ 2.5 nm does not make them 'too small' to be able to act as excellent catalysts.

It was therefore intriguing to us to read that PO_4^{3-} ions significantly inhibit the radical scavenging ability of CNPs, and we thus decided to expand our programme by exploring more generally the effect of P-based ligands on the resulting nuclearity, structure, and catalytic ability of any obtained products. We herein report the isolation of two Ce/O clusters from this work and their $HO^{\bullet}$ radical scavenging ability as monitored by a UV/vis study.

Experimental Section

Syntheses

All manipulations were performed under aerobic conditions using chemicals and solvents as received, unless otherwise stated; py = pyridine.

$(pyH)_8[Ce_{10}O_4(OH)_4(O_3PPh)_{12}(NO_3)_{12}]$ (1). $PhPO_3H_2$ (0.079 g, 0.50 mmol) and $^tBuCO_2H$ (0.10 g, 1.0 mmol) were dissolved in a stirred solution of py:MeOH (10:1 mL) followed by addition of $(NH_4)_2[Ce(NO_3)_6]$ (0.55 g, 1.0 mmol). Stirring was continued for a further 30 min and then the yellow solution was layered with EtOH (20 mL) and left to stand undisturbed for 5 days at ambient temperature, during which time yellow block crystals of **1**·xEtOH suitable for single-crystal X-ray crystallography slowly formed. Crystals for X-ray studies were maintained in mother liquor, otherwise they were filtered, washed with EtOH, and dried under vacuum. The yield was 54 mg, 27 % based on P. Anal. Calcd (found) for **1** (solvent free; $C_{112}H_{112}Ce_{10}N_{20}O_{80}P_{12}$): C 28.08 (27.62); H 2.36 (2.67); N 5.85 (5.74). Selected IR data (cm^{-1}): 3134 (br), 1387 (s) 1314 (m), 1136 (s), 1084 (s), 1025 (s), 974 (s), 825 (s), 752 (ss), 680 (m), 607 (w), 559 (w), 528 (m), 444 (w).

$[Ce_6O_4(OH)_4(O_2PPh_2)_4(O_2C^tBu)_8]$ (2). Ph_2PO_2H (0.11 g, 0.50 mmol) and $^tBuCO_2H$ (0.10 g, 1.0 mmol) were dissolved in a stirred solution of py:MeOH (10:1 mL) followed by addition of $(NH_4)_2[Ce(NO_3)_6]$ (0.55 g, 1.0 mmol). Stirring was continued for a further 30 min and then the yellow solution was layered with MeCN (20 mL) and left to stand undisturbed for 5 days at ambient temperature, during which time yellow triangular prisms of **2**·2py·$2H_2O$ slowly crystallized. Crystals for single-crystal X-ray crystallography were maintained in mother liquor, otherwise they were filtered, washed with MeCN, and dried under vacuum. The yield was 116 mg, 32 % based on P. Anal. Calcd (found) for **2**·2py·$2H_2O$ ($C_{98}H_{130}Ce_6N_2O_{34}P_4$): C 41.38 (41.14); H 4.61 (4.44); N 0.98 (0.90). Selected IR data (cm^{-1}): 3416 (br), 2955 (w), 1441 (s), 1224 (s), 1122 (s), 1038 (s), 1019 (s), 753 (m), 730 (m), 696 (m), 579 (m), 553 (s), 527 (s), 467 (w).

$[Ce_6O_4(OH)_4(O_2C^tBu)_{12}]$ (3). $Ce(NO_3)_3$ (0.22 g, 0.50 mmol) was dissolved with stirring in MeCN (15 mL) followed by addition of $^tBuCO_2H$ (0.12 g, 1.2 mmol) and py (360 μL, 4.4 mmol). The mixture was stirred for an hour and then $(NH_4)_2[Ce(NO_3)_6]$ (0.055 g, 0.10 mmol) was added to the colorless solution. The resulting yellow solution was stirred for another hour and then left to stand undisturbed at ambient temperature for 14 days, during which time small gold crystals slowly grew. The yield was 90 mg, 40% based on Ce. Anal. Calcd (found) for **3**·$^2/_3$MeCN·$2H_2O$ ($C_{61.33}H_{118}Ce_6N_{0.67}O_{34}$): C 32.75 (32.68); H 5.29 (5.26); N 0.42 (0.41). Selected IR data (cm^{-1}): 3644 (s), 2960 (s), 2928 (w), 2871 (m), 1547 (s, br), 1484 (s), 1417 (s), 1375 (s), 1360 (s), 891 (m), 782 (m), 630 (m), 584 (s), 529 (s), 400 (s, br).

Physical Measurements

Infrared spectra were recorded in the solid state (KBr pellets) on a Nicolet Nexus 670 FTIR spectrometer in the 400-4000 cm^{-1} range. All FTIR spectra were processed by Spectragryph: Optical Spectroscopy Software.[27] Elemental analyses (C, H, and N) were performed by Atlantic Microlabs, Inc. UV/vis spectra for **1–3** were obtained on solutions in DMF in the 270 - 800 nm range on an Evolution 201 spectrophotometer with the temperature maintained at 25 °C with a PCCU1 module.

X-ray Crystallography

Crystal data and structure refinement parameters for complexes **1**·xEtOH and **2**·2py·$2H_2O$ are listed in Table 1. The crystals showed signs of deterioration at 100 K and were thus maintained at 233 K for data collection. X-ray intensity data were collected on a Bruker DUO diffractometer using MoK_α radiation (λ = 0.71073 Å) and an APEXII CCD area detector. X-Ray intensity data for **3** were collected on a Bruker Dual micro source D8Venture diffractometer and PHOTON III detector running APEX3 software package of programs and using MoK_α radiation (λ = 0.71073 Å). Raw data frames were read by program SAINT and integrated using 3D profiling algorithms.[28] The resulting data were reduced to produce hkl reflections and

their intensities and estimated standard deviations. The data were corrected for Lorentz and polarization effects and numerical absorption corrections were applied based on indexed and measured faces.

The structures were solved and refined in *SHELXTL2014*, using full-matrix least-squares cycles.[29] The refinement was carried out by minimizing the wR_2 function using F^2 rather than F values. R_1 is calculated to provide a reference to the conventional R value but its function is not minimized. All non-H atoms were refined with anisotropic thermal parameters; all H atoms were placed in calculated idealized positions and refined riding on their parent atoms.

1·xEtOH was solved and refined in space group $P\bar{4}3m$ and consists of a Ce_{10} cluster anion located on $\bar{4}3m$ centers, thus only 1/24 of it is in the asymmetric unit. The latter contains two Ce atoms at sites of eight-fold multiplicity for Ce1 and six-fold multiplicity for Ce2, two O^{2-} ligands O1 and O2, and half a $PhPO_3^{2-}$ ligand. Ce2 has three NO_3^- ligands but the six-fold symmetry means that they are disordered over six positions. All the phenyl rings are disordered and were refined in two positions with their site occupation factors fixed at 50% due to symmetry. The two pyH^+ cations and an estimated twelve 12 alcohol solvent molecules were badly disordered and could not be modelled properly, thus program SQUEEZE,[30,] a part of the PLATON package of crystallographic software,[31] was used to calculate the cation/solvent disorder area and remove its contribution to the overall intensity data.

Table 1. Crystal data and structure refinement details for **1** and **2**

	1·xEtOH	**2**·2py·2H_2O
Formula [a]	$C_{112}H_{112}Ce_{10}N_{20}O_{80}P_{12}$	$C_{98}H_{126}N_2Ce_6O_{34}P_4$
Fw, g mol^{-1} [a]	4790.85	2888.64
Space group	$P\bar{4}3m$	I4/m
a, Å	15.9001(4)	15.4524(7)
b, Å	15.9001(4)	15.4524(7)
c, Å	15.9001(4)	25.1756(11)
α, °	90	90
β, °	90	90
γ, °	90	90
V, $Å^3$	4019.8(3)	6011.3(6)
Z	1	2
T, K	233 (2)	233 (2)
λ, Å [b]	0.71073	0.71073
$\rho_{calc,}$ g cm^{-3}	1.941	1.596
μ, mm^{-1}	2.993	2.350
*R*1 [c, d]	0.0360	0.0456
*wR*2 [e]	0.1038	0.1235

[a] Solvent molecules excluded for **1** and included for **2**. [b] Graphite monochromator. [c] $I > 2\sigma(I)$. [d] $R1 = \Sigma(||F_O| - |F_C||) / \Sigma|F_O|$. [e] $wR2 = [\Sigma[w(F_O^2 - F_C^2)^2] / \Sigma[w(F_O^2)^2]]^{1/2}$, $w = 1/[\sigma^2(F_O^2) + (m*p)^2 + n*p]$, $p = [\max(F_O^2,0) + 2*F_C^2]/3$, m and n are constants.

Even though counterions were not located definitively by crystallographic means, they were concluded from elemental analysis to be 8 pyH^+ groups. They are believed to reside four-each in two locations of highly-disordered electron density: the first is around a $\bar{4}3m$ symmetry center near the three disordered NO_3^- ligands where a large collection of electron density has a multiplicity of 24. The second is a collection of electron density at 0 ½ ¼, a $\bar{4}2m$ symmetry position with multiplicity of 24, lying in a void between the other collection of electron density and the Ce_{10} cation cluster. The data were refined as a perfect/merohedral twin. In the final cycle of refinement, 1794 reflections (of which 1604 are observed with $I > 2\sigma(I)$) were used to refine 63 parameters, and the resulting R_1, wR_2 and S (goodness of fit) were 3.60 %, 10.38 % and 1.166, respectively.

For complex **2**·2py·2H_2O, the asymmetric unit consists of $^1/_8$ of the Ce_6 cluster lying on a 4/m symmetry position, and $^1/_4$ each of py and H_2O solvent molecules. Thus, the Ce_6:py:H_2O ratio is 1:2:2. Both the Me groups of $^tBuCCO_2^-$ ligands and Ph rings of $Ph_2PO_2^-$ ligands were disordered about two positions with 50% occupancies. All solvent molecules were disordered and could not be modelled properly, thus program SQUEEZE was again used to calculate the solvent disorder area of two py and two H2O and remove its contribution to the overall intensity data. In the final cycle of refinement, 3553 reflections (of which 2624 are observed with $I > 2\sigma(I)$) were used to refine 127 parameters and the resulting R_1, wR_2 and S were 4.56 %, 12.35 % and 1.044, respectively.

$[Ce_6O_4(OH)_4(O_2C^tBu)_{12}]$ has been previously reported from a different procedure,[32] and present complex **3** was concluded to be the same compound from a unit cell determination ($a = b$ = 22.0653 Å, c = 15.3810 Å, $\alpha = \beta$ = 90°, γ = 120°, V = 6485.4 $Å^3$, T = 233 K) that matched the unit cell of the previous report ($a = b$ = 21.8220(4) Å, c = 15.2295(6) Å, $\alpha = \beta$ = 90°, γ = 120°, V = 6280.7(3) $Å^3$, T = 100 K).

UV/vis Radical Scavenging Studies

Samples for radical scavenging studies comprised 90 μM H_2O_2, 20 μM methylene blue (MB), 10 μM Ce/O cluster, 45 μM $FeCl_2$, and the final volume of the solution was adjusted to 3.0 mL. To ensure that the Ce/O cluster solution would contain an equal dispersion of sample within the solution, compounds were ground before being added to the water and shaken prior to addition to the UV/vis cell. The $FeCl_2$ was added last to generate the $HO^•$. On addition of the $FeCl_2$ a timer was started, and the sample was shaken before being transferred to the UV/vis spectrometer. A scan in the 180–800 nm was taken immediately and recorded as 0 s, and then again at 10 mins. The same experimental procedure was followed to monitor the absorbance of the MB at 666 nm at 30 s intervals for a total time course of 10 min. For the control experiments, the oxidation of MB in the absence of the Ce/O cluster, the same procedure was followed with the exception that the addition of Ce/O cluster was replaced with an equal volume of H_2O. Measurements were performed in triplicate to allow for determination of the standard deviation.

Results and Discussion

Syntheses

Organophosphonates (RPO_3^{2-}) and diorganophosphinates ($R_2PO_2^-$) have been widely used in transition metal cluster chemistry owing to their ability to bridge multiple metals and thus form polynuclear complexes with a wide range of interesting structures and applications from catalysis to molecular magnetism.[33] Our own group's first employment of the common $Ph_2PO_2^-$ was as a 'pseudo-carboxylate' to prepare the mixed-ligand $[Mn_{12}O_{12}(O_2CR)_{16-x}(Ph_2PO_2)_x(H_2O)_4]$ (x = 7, 8) single-molecule magnets by carboxylate substitution reactions on the parent $[Mn_{12}O_{12}(O_2CR)_{16}(H_2O)_4]$.[34,35] We thus used the same mixed-ligand strategy in our search for Ce/O clusters with phosphorus-based ligands. We explored a variety of RCO_2H reagents in reactions involving $PhPO_3H$ or Ph_2PO_2H,[33] but only pivalic acid ($^tBuCO_2H$) led to pure, isolable products, even though **1** turned out not to contain any $^tBuCO_2^-$ ligands.

1 and **2** were isolated from similar reactions of $(NH_4)_2[Ce(NO_3)_6]$ with $PhPO_3H$ or Ph_2PO_2H, respectively, and $^tBuCO_2H$ in a 2:1:2 molar ratio in py:MeOH (10:1 v/v). Layering of the reaction solutions with EtOH or MeCN led to isolation of well-formed crystals of pure compounds in non-optimized yield of 27 and 32 % yield, respectively. These layering solvents were found to give the best crystals, suitable for crystallography. Since $^tBuCO_2^-$ is not incorporated into the ligand shell of **1**, the reaction was repeated in the absence of the $^tBuCO_2H$. The isolated product was shown by IR spectral comparison to be different from **1**, but we were unable to obtain suitable crystals for its structural characterization. Nevertheless, this result showed that although $^tBuCCO_2^-$ is not incorporated, its presence is required to give pure **1**. Attempts to obtain higher nuclearity products by varying reaction times, temperature, and carboxylate identity have all been unsuccessful to date.

Complex **3** has been previously obtained in 13 % yield from the reaction of $Ce(NO_3)_3$, $[Cu_2(H_2O)(O_2C^tBu)_4(^tBuCO_2H)_4]$, and diethanolamine in MeCN.[32] It was also obtained in 22% yield from the reaction of $Ce(NO_3)_3$, $[Mn(O_2CMe)_2$, propane-1,3-diol, and $^tBuCO_2H$ in MeCN.[32] From prior experience, we felt that we could develop a more rational synthesis,[24] and we accomplished this from the reaction of $Ce(NO_3)_3$, $^tBuCO_2H$, py, and $(NH_4)_2[Ce(NO_3)_6]$ in MeCN in a yield of 40 %.

Structural Descriptions

The smallest reasonable unit of the fluorite lattice of CeO_2 is the Ce_6 octahedron, and this has been isolated in the past with a number of ligation environments.[32,36–41] It is interesting to note that all three of the complexes in the present work, **1-3**, contain a Ce_6 octahedral core.

1·xEtOH crystallizes in cubic space group $P\bar{4}3m$ with only two Ce ions in the asymmetric unit. The Ce_{10} anion thus has crystallographic T_d point group symmetry, if the Ph ring and NO_3^- disorders are ignored. From the viewpoint of Fig. 1 (top) the vertical axis is a C_2 symmetry element. The core consists of a $\{Ce^{IV}_6(\mu_3\text{-}O)_4(\mu_3\text{-}OH)_4\}$ face-capped octahedron with four additional Ce^{IV} ions each linked to the octahedron via three μ_3-$PhPO_3^{2-}$ ligands forming a super-tetrahedron, i.e., a Ce_6 octahedron within a concentric Ce_4 tetrahedron (Fig. 1). Each $PhPO_3^{2-}$ bridges a Ce_2 edge of the octahedron with two of its O atoms and attaches to an outer Ce with its third one (Scheme). Peripheral ligation is completed by three chelating NO_3^- ligands on each outer Ce, which are nine-coordinate. Similar super-tetrahedral cores have been observed multiple times in, for example, Mn/O chemistry, but in those cases the outer Mn are directly attached to the core μ_3-O^{2-} ions making them μ_4.[42–44]

The O^{2-} : OH^- = 4:4 in the core of **1** is also the usual situation in previous Ce_6 octahedra, but O^{2-} : OH^- = 5:3 is also known,[39] as is an 8:0 example.[41] There is usually O^{2-}/OH^- disorder, but not in **1**, likely due to the external Ce^{IV} ions lying not far from the μ_3-O^{2-} ions (O2) and thus disfavoring their protonation. The ordered O^{2-}/OH^- situation can be seen in the resulting O coordination geometries, even though the H atoms were not located, with the four μ_3-OH ions (O1) being distinctly more pyramidal, consistent with them being four-coordinate distorted tetrahedral. This also shows up in the Ce-O/Ce-O-Ce bond lengths/angles, which are 2.405(7)Å/104.1(4)° and 2.220(3)Å/117.4(2)° for the OH^- and O^{2-} ions, respectively. As a result, the OH^- and O^{2-} ions are 0.996(6) and 0.363(6) Å, respectively, above the Ce_3 faces that they bridge.

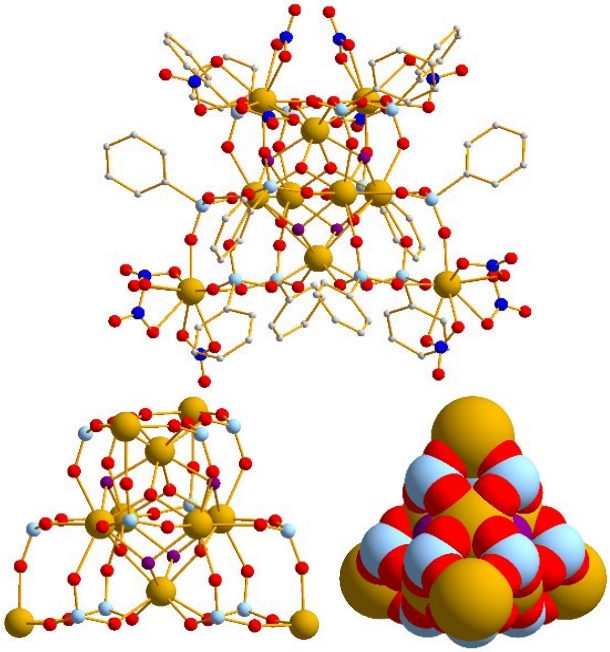

Fig. 1. The Ce_{10} anion of **1**. (**top**) The complete structure excluding H atoms and ligand disorder. (**bottom left**) The Ce_{10} unit without Ph rings and NO_3^- ligands, slightly rotated about the vertical C_2 axis compared to the top. (**bottom right**) The Ce_{10} unit without Ph groups and NO_3^- ligands in space-filling mode from a viewpoint that emphasizes the outer Ce_4 tetrahedron. Atom colour code: Ce^{IV} gold, O red, OH purple, P sky blue, N blue, and C grey.

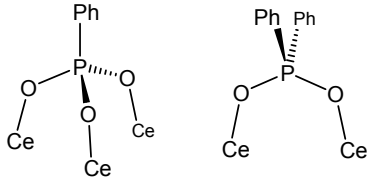

$\eta^1{:}\eta^1{:}\eta^1{:}\mu_3$ $\eta^1{:}\eta^1{:}\mu$

Scheme

We have previously demonstrated the utility of bond valence sum (BVS) calculations for determining the oxidation states of Ce ions and the protonation level of O atoms in molecular nanoparticles of CeO_2.[45,46] For the anion of **1**, BVS calculations (Table 2) confirm that all Ce ions are in the +4 oxidation state and that there are four O^{2-} and four HO^- present and ordered in the core octahedron, giving an overall charge for the anion of **1** of 8−.

2·2py·2H_2O crystallizes in tetragonal space group $I4/m$ with two Ce ions in the asymmetric unit. The complex has crystallographic D_{4h} symmetry. The complete structure is shown in Fig. 2 with a C_2 symmetry element as the vertical axis. The core consists of a Ce_6 octahedron with a μ_3-O bridging each face and peripheral ligation provided by eight $tBuCO_2^-$ and four $Ph_2PO_2^-$ groups each bridging a Ce_2 edge in the common syn,syn η^1:η^1:μ-bridging mode. The four $Ph_2PO_2^-$ groups all lie in the horizontal mirror plane of the D_{4h} structure possibly to avoid the steric effects from the bulky –PPh_2 units. Overall, **2** is similar to other Ce_6 clusters in the literature but the first discrete one with P-based ligation.[32,38–41] Charge considerations indicate a quadruply-protonated $\{Ce^{IV}_6(\mu_3\text{-}O)_4(\mu_3\text{-}OH)_4\}$ core as in **1**, but with O^{2-}/OH^- disorder due to the high crystallographic D_{4h} symmetry. The Ce^{IV} oxidation states and O^{2-}/OH^- protonation levels were generally confirmed by BVS calculations (Table 2), although the disorder affected somewhat the obtained numbers due to averaging of the O^{2-}/OH^- positions (whose O atoms would be in slightly different positions, as in **1**) and thus the apparent Ce-O distances used in the BVS calculations. As a result the BVS values of Ce1 and Ce2 in **2**, 3.67 and 3.47, respectively, are lower than would be expected for a Ce^{IV} ion (Table 2).[45,46] Similarly, the BVS value of the core O atoms, O1, is 1.47, intermediate between O^{2-} and OH^- values and supporting disorder between them. The possibility that the low Ce BVS was due to the presence of one or more Ce^{III} ions in a disordered $Ce^{III}_xCe^{IV}_{6-x}$ octahedron masked by symmetry, as we have previously seen in a Ce_{24} cluster[24] would be highly unusual as all previous Ce_6 species have contained exclusively Ce^{4+} ions.[38–40] Nevertheless, to probe this further an electron paramagnetic resonance (EPR) spectrum was taken of **2**·2py·2H_2O (Fig. S1), but the only signal observed was a weak signal from the Cu resonator of the instrument also present in the blank. Since strong EPR signals have been observed previously when Ce^{III} ions have been present in other Ce/O clusters such as Ce_{24a} (Fig. S1),[23,24] we conclude that **2** is indeed a Ce^{IV}_6 complex with a $\{Ce_6O_4(OH)_4\}$ core.

Table 2. BVS values for core Ce and O atoms for **1** and **2**

	Atom	Ce^{III}	Ce^{IV}	CN	Atom[c]	BVS	Ion
1	Ce1	4.49	**3.94** [b]	8	O1	1.21	OH^-
	Ce2	4.71	**4.13** [b]	9	O2	2.00	O^{2-}
2	Ce1	4.18	**3.67** [a,b]	8	O1	1.47[d]	O^{2-}/OH^-
	Ce2	3.96	**3.48** [a,b]	8			

[a] The bold values for Ce are the ones closest to the charge for which they were calculated; the oxidation state is thus the nearest integer to the bold value. [b] See text. [c] An O BVS in the ~1.8-2.0, ~0.9-1.2, ~0.- 0.4 range indicates non-, single- and double-deprotonation, respectively. [d] Intermediate values in the range ~1.50–1.70 are assigned to 1:1 O^{2-}/OH^- crystallographic disorder; see the text.

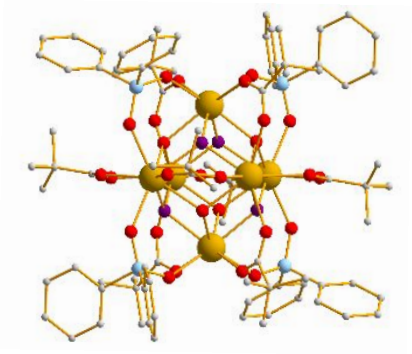

Fig. 2 The complete structure of **2** excluding H atoms. The C_4 axis is in the horizontal plane and a C_2 axis is vertical. Disordered O^{2-}/OH^- ions in the core are shown as ordered for convenience. Atom colour code: Ce^{IV} gold, O red, OH purple, P sky blue and C grey.

The identity of **3** was confirmed as the known $[Ce_6O_4(OH)_4(O_2C^tBu)_{12}]$ by unit cell and FT-IR spectral comparisons with the published material.[32] It is the all-$^tBuCO_2^-$ version of **2**, and also shows O^{2-}/OH^- disorder.

UV/vis Spectral Studies

The UV/vis spectra of **1**-**3** were recorded in dimethyl formamide (DMF) to assess whether they would interfere with the studies below, and the obtained spectra are shown in Fig. 2. The complexes exhibit somewhat different absorption profiles, and none of them shows significant absorption above ~500 nm or so; there are no other features in the 550-800 nm range. Phosphorus-containing **1** and **2** exhibit similar profiles and noticeably different from that of **3**, with a greater absorption in the 320-350 range. In particular, the different profiles of **2** and **3**, even though they are of identical nuclearity and core structure, and both have mainly or completely $^tBuCO_2^-$ligation, indicate the effect the $Ph_2PO_2^-$ ligands have on the optical properties of **2**.

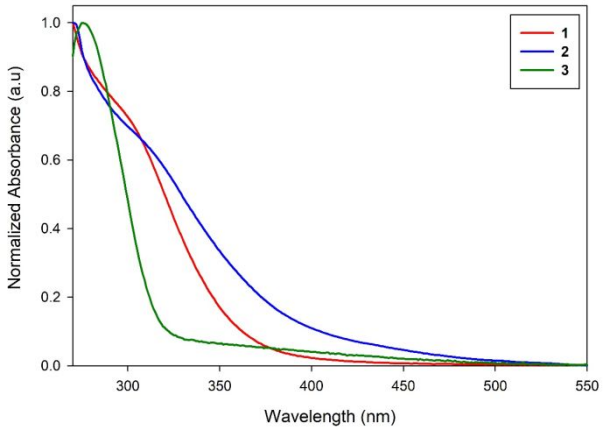

Fig. 3. UV/vis spectra of complexes 1-3 in DMF solution. The spectra were measured between 270 – 800 nm and are shown between 270 – 550 nm.

Radical Scavenging Studies

Chromogenic molecules have been widely used to follow oxidation reactions, wherein a redox event on the chromogenic molecule leads to an observable colour change to the solution and a corresponding change in its UV/vis spectrum. Likewise, these molecules allow for the study of chemical agents that could inhibit the oxidation of the chromogenic molecules, so-called antioxidants. For example, the chromogenic methyl violet (MV) can be oxidized by HO• radicals generated by the Fenton reaction (Eq 1), but this oxidation of MV may be hindered or completely suppressed by the addition of a radical scavenger to

$$Fe^{2+} + H_2O_2 \longrightarrow Fe^{3+} + HO^- + HO^\bullet \qquad (1)$$

the reaction solution, providing a means for investigating radical scavenging ability.[47–50] One such class of antioxidant are CNPs: when employed in a MV solution exposed to hydroxyl radicals, it was found that CNPs with a high concentration of Ce^{3+} ions were able to efficiently scavenge the radicals and prevent its oxidation.[47-49]

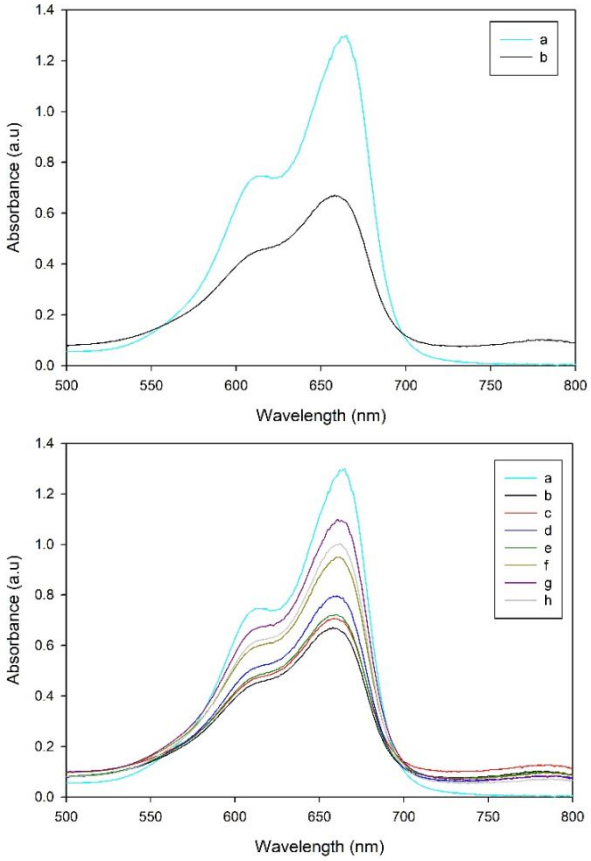

Fig. 4. The hydroxyl radical scavenging ability of Ce/O clusters monitored by UV/vis spectroscopy. **(top)** (a) The spectrum of methylene blue (MB) alone, and (b) after incubation with HO• radicals for 10 mins. **(bottom)** (a and b) The spectra from the top figure, and (c - h) after incubation with HO• radicals for 10 mins in the presence of Ce/O clusters. Legend code: (a) MB alone; (b) H_2O_2/MB/Fe^{2+}; (c) H_2O_2/MB/**1**/Fe^{2+}; (d) H_2O_2/MB/**2**/Fe^{2+}; (e) H_2O_2/MB/**3**/Fe^{2+}; (f) H_2O_2/MB/$\mathbf{Ce_{24a}}$/Fe^{2+}; (g) H_2O_2/MB/$\mathbf{Ce_{24b}}$/Fe^{2+}; (h) H_2O_2/MB/$\mathbf{Ce_{38}}$/Fe^{2+}.

Similar studies have been conducted with other chromogenic molecules. For example, methylene blue (MB), displays a strong absorbance peak at ~660 nm ($n\rightarrow\pi^*$), the intensity of which decreases as it is oxidized.[51] There is another strong absorbance centered at ~610 nm from the 0→1 vibronic transition.[52] It has been shown that hydroxyl radicals can oxidize MB (Fig. 3),[53,54] making it an ideal candidate to examine the radical scavenging ability of Ce/O clusters. Previous investigations into catalytic HO• radical scavenging by Ce/O molecular nanoparticles showed that under the experimental conditions employed the best scavengers usually had a low Ce^{3+}: Ce^{4+} ratio, suggesting that **1-3**, each comprised of only Ce^{4+} ions, might be good hydroxyl radical scavengers. However, since **1** and **2** are the first Ce/O clusters with P-based ligands, they might instead prove poor scavengers, analogous to the poor scavenging ability of CNPs in the presence of PO_4^{3-}, as mentioned in the Introduction. Thus, to allow for comparisons with other Ce/O molecular nanoparticles, the HO• scavenging ability of the $[Ce_{24}O_{28}(OH)_8(O_2CPh)_{30}(py)_4]$ (Ce_{24a}), $[Ce_{24}O_{27}(OH)_9(O_2CPh)_{30}(py)_4]$ (Ce_{24b}) and $[Ce_{38}O_{54}(OH)_8(O_2CEt)_{36}(py)_8]$ (Ce_{38}) clusters,[23,24] which contain 2, 3 and 0 Ce^{III} ions, respectively, on their core surface, were also assessed under the same conditions as **1**-**3**.

The UV/vis spectral changes for MB with HO• radicals in the presence and absence of Ce/O clusters are shown in Fig. 4. The control spectra in Fig. 4, top, show that after 10 mins exposure of MB to HO• radicals the initially stable spectrum (a) decreases significantly (b) and a new feature appears centered at 782 nm, likely due to an oxidation product of MB. As a further control, we investigated the possible pro-oxidant ability of the six complexes, i.e., whether in the absence of the Fe^{2+} salt they can generate HO• radicals from H_2O_2 and thus cause oxidation of the MB and a lowering of its absorbance. For all six compounds, we found that the absorbance of the MB remains constant over the 10-minute measurement period, and thus we conclude they exhibit no pro-oxidant activity.

We next generated HO• from the Fenton reaction in the presence of Ce/O clusters, and it is evident that the latter exhibit varying ability to protect the MB from HO• (Fig. 4, bottom). The absorbance of MB after 10 minutes of incubation with HO• remains at its greatest for Ce_{24b} and the least for **1**. Thus, Ce_{24b} is the best HO• scavenger assessed under these conditions, catalytically scavenging HO• so efficiently that it allows little attack on MB. In fact, Ce_{24a}, Ce_{24b}, and Ce_{38} are all significantly better than **1**-**3**, which are all poor. We also monitored the time course of the reactions, and the results (Fig. 5) show that the separation of scavenging ability into two groups is evident almost from time zero, and thus is not due, for example, to decomposition of some clusters to give less or more active products, which might cause some of the plots to cross. Instead, throughout the 10 mins the order of scavenging ability remains $Ce_{24b} > Ce_{38} > Ce_{24a} >$ **2** ≈ **3** > **1**.

For future Ce/O cluster and molecular nanoparticle radical scavenging studies, we propose a simple quantification of the results that will allow for facile comparison of radical scavenging ability. This is shown in Eq 2, where *P* is the % protection of the

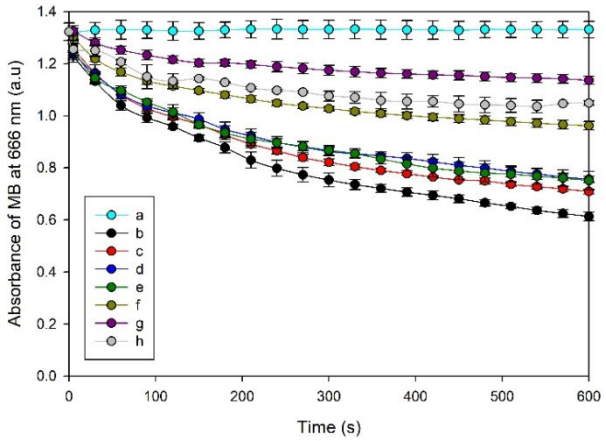

Fig. 5. Time course of the decay of the MB spectrum due to reaction with HO• radicals, monitored by the peak absorbance at ~660 nm, in the absence or presence of Ce/O clusters. Legend code: (a) MB; (b) MB/ H_2O_2/Fe^{2+}; (c) MB/H_2O_2/**1**/Fe^{2+}; (d) MB/**2**/H_2O_2/Fe^{2+}; (e) MB/**3**/H_2O_2/Fe^{2+}; (f) MB/**Ce_{24a}**/H_2O_2/Fe^{2+}; (g) MB/**Ce_{24b}**/H_2O_2/Fe^{2+}; (h) MB/**Ce_{38}**/H_2O_2/Fe^{2+}.

$$P = 100 - 100(\Delta A/\Delta A_0) \quad (2)$$

MB (or other chromogenic molecule), ΔA is the decrease in the MB absorbance in the presence of Ce/O cluster or other radical scavenger, and ΔA_0 is the decrease in the MB absorbance in the absence of Ce/O cluster. Thus, *P* correlates with radical scavenging ability, and $\Delta A/\Delta A_0$ is the fraction of chromogenic molecule oxidized in the presence vs absence of Ce/O cluster or other scavenger. Using Eq 2, the scavenging ability of the six Ce/O clusters in this work is shown in Fig. 6, and it clearly emphasizes the separation into two groups.

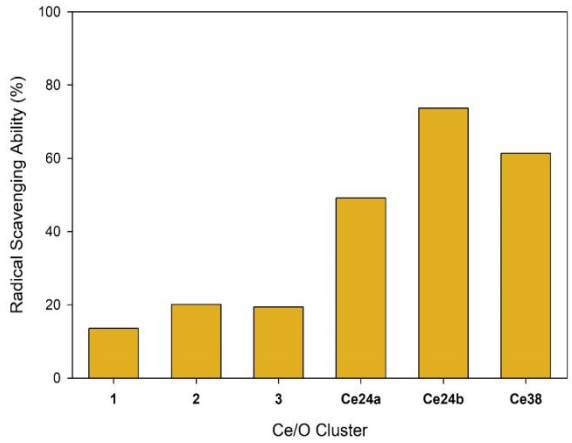

Fig. 6. The HO• radical scavenging ability (*P*, %) of the six assessed Ce/O clusters calculated using Eq 2 at a reaction time of 10 mins. Conditions: H_2O_2 (90 μM), Ce/O (10 μM), MB (20 μM) and Fe^{2+} (45 μM).

The poor radical scavenging ability of **1**-**3** is interesting but difficult to unequivocally rationalize. For **1** and **2** it parallels the reduced scavenging ability of CNPs in the presence of PO_4^{3-} ions, [20–22] which were proposed to bind to the surface, and the present work with related P-based ligands $PhPO_3^{2-}$ and $Ph_2PO_2^-$ would support this explanation. How this decreases the radical scavenging activity, however, is not clear, although at least three obvious possibilities come to mind: (i) The organic shell of bulky R- groups of the P-based and/or $^tBuCO_2^-$ ligands of **1**-**3** is efficiently enveloping the core and preventing access by the HO• radicals to the Ce/O surface; (ii) it could be that the small size of **1**-**3** compared to the larger Ce/O molecular nanoparticles investigated in this work makes them intrinsically poorer catalysts for radical scavenging; and (iii) some other effect is important, such as changes to the Ce^{III}/Ce^{IV} redox potentials hindering their redox cycling for radical scavenging catalysis.

For (i), examination of the structures of the anion of **1** and **2** in space-filling mode reveals that access to the surface is not completely closed off by the bulky ligands employed (Fig. S2), which argues against this being the main explanation for their poor radical scavenging ability. The similarities between **2** and **3** suggest this is also the case for **3**. In addition, it has been found that CNPs with a shell of surfactants such as oleic acid[55] or encased in polymer vesicles[56] were still able to effectively scavenge ROS. For (ii), previous studies have shown that activity does not correlate simply with nuclearity even down to Ce_6, and specifically the corresponding 2,6-dimethoxybenzoate version of **3**, i.e., $[Ce^{IV}_6O_4(OH)_4(O_2CC_6H_3\text{-}2,6\text{-}Me_2)_{12}]$, is an excellent catalytic scavenger of HO• radicals.[24] For (iii), the nature of the ligand shell could certainly affect the Ce^{III}/Ce^{IV} redox potentials and thus the ability of the Ce ions to redox cycle, so this could be a contributing factor to the reduced activity of **1**-**3** compared to Ce_{24a} and Ce_{24b}, which contain $PhCO_2^-$/py ligands, and Ce_{38} which contains $EtCO_2^-$/py. It would also help rationalize the big difference in scavenging ability between Ce_6 complexes **2**/**3** and the previously studied $[Ce^{IV}_6O_4(OH)_4(O_2CC_6H_3\text{-}2,6\text{-}Me_2)_{12}]$. In addition, binding of highly charged PO_4^{3-} groups to the surface of CNPs would be expected to favor the Ce^{IV} oxidation state, i.e., make reduction of surface Ce^{IV} to Ce^{III} more difficult, and such an effect may also be contributing here, especially for the $PhPO_3^{2-}$-containing complex **1**. The bottom line is that multiple factors are probably contributing to determining the catalytic scavenging ability of molecular Ce/O clusters.

The results described herein for Ce_{24a} and Ce_{38} are consistent with those reported by Mitchell *et al*.,[24] which were monitored by EPR spectral intensity of a spin trap and showed that both complexes are good scavengers but with Ce_{38} (no Ce^{III} ions) slightly better than Ce_{24a} (2 Ce^{III} ions). What is, however, surprising is the high scavenging ability of Ce_{24b} (3 Ce^{III} ions), which is in notable contrast to its poor activity in the previous work. We note that the experimental conditions necessitated by the two studies were somewhat different, such as the different ratios of H_2O_2:Fe^{2+} in the present and previous work of 2:1 and 1:1, respectively, and higher concentrations of both species in the previous work, but since these should only affect the amount of HO• radicals produced[49] it is not clear why such differences would selectively affect Ce_{24b} so much. The bottom line is that there are clearly multiple factors at play, and this is another reason that the radical scavenging ability of molecular nanoparticles must be compared under exactly the same conditions, as in the present study.

Conclusions

Using procedures similar to those reported by Mitchell *et al,*.[23,24] the presence of phosphorus-based reagents has led to isolation of two Ce/O clusters with the P-based groups in their ligand shell. The first conclusion of this work is thus that P-based ligands can be incorporated for the first time into Ce/O clusters. However, the nuclearities of **1** and **2** are low, both containing a Ce_6 unit, the smallest unit of the CeO_2 fluorite lattice, with **1** also possessing four additional Ce ions on the periphery of the core, held there by the $PhPO_3^{2-}$ groups whose strong, tridentate binding within **1** is likely the reason the nuclearity does not get larger. This is in contrast to the usual case with corresponding benzoates and other carboxylates, the former favouring Ce_{24} products, for example. In contrast, the $Ph_2PO_2^-$ groups are binding in the same common $\eta^1{:}\eta^1{:}\mu$ bridging mode as carboxylates, and the low nuclearity of **2** is therefore assigned to the bulk of these hindering nuclearity growth.

Regardless of the low nuclearities, a major aim of this work was to assess the radical scavenging ability of any Ce/O clusters that might be obtained with P-containing ligands, and **1** and **2** have been found to be poor catalysts of $HO^{\bullet}$ radical scavenging as monitored by UV/vis of MB oxidation. This is consistent with the observation in the CNP literature that PO_4^{3-} inhibits their radical scavenging ability, but the precise reason is unclear. For future design of Ce/O molecular nanoparticles for the purpose of $HO^{\bullet}$ or other radical scavenging it is clear that the ligand shell is an important parameter to consider, and phosphorus-based ligands would seem to offer no advantages since they seem to inhibit radical-scavenging ability of systems that with all-carboxylate ligation are excellent scavengers.

Acknowledgements

We thank the NSF for funding this work through grant CHE-1900321, and for the purchase of the X-ray diffractometer through grant CHE-1828064.

Conflicts of interest

There are no conflicts to declare.

Notes and references

1 M. Flytzani-Stephanopoulos, *MRS Bulletin*, 2001, **26**, 885–889.
2 A. Trovarelli, *Catalysis Reviews*, 1996, **38**, 439–520.
3 A. Trovarelli, C. de Leitenburg, M. Boaro and G. Dolcetti, *Catalysis Today*, 1999, **50**, 353–367.
4 C. Sun, H. Li and L. Chen, *Energy Environ. Sci.*, 2012, **5**, 8475–8505.
5 K. Reed, A. Cormack, A. Kulkarni, M. Mayton, D. Sayle, F. Klaessig and B. Stadler, *Environmental Science: Nano*, 2014, **1**, 390–405.
6 M. Perullini, S. Bilmes, M. Jobbagy, R. Brayner, F. Fievet and T. Coradin, in *Nanomaterials: A Danger or a Promise?*, 2012, pp. 307–334.
7 C. Walkey, S. Das, S. Seal, J. Erlichman, K. Heckman, L. Ghibelli, E. Traversa, J. F. McGinnis and W. T. Self, *Environ. Sci.: Nano*, 2015, **2**, 33–53.
8 S. Kargozar, F. Baino, S. J. Hoseini, S. Hamzehlou, M. Darroudi, J. Verdi, L. Hasanzadeh, H.-W. Kim and M. Mozafari, *Nanomedicine*, 2018, **13**, 3051–3069.
9 J. Kailashiya and D. Dash, *Annals of the National Academy of Medical Sciences (India)*, 2019, **55**, 014–017.
10 N. Thakur, P. Manna and J. Das, *Journal of Nanobiotechnology*, 2019, **17**, 84.
11 A. S. Karakoti, N. A. Monteiro-Riviere, R. Aggarwal, J. P. Davis, R. J. Narayan, W. T. Self, J. McGinnis and S. Seal, *JOM (1989)*, 2008, **60**, 33–37.
12 S. Das, J. M. Dowding, K. E. Klump, J. F. McGinnis, W. Self and S. Seal, *Nanomedicine*, 2013, **8**, 1483–1508.
13 C. Xu and X. Qu, *NPG Asia Mater*, 2014, **6**, e90.
14 B. C. Nelson, M. E. Johnson, M. L. Walker, K. R. Riley and C. M. Sims, *Antioxidants*, 2016, **5**, 15.
15 M. Das, S. Patil, N. Bhargava, J.-F. Kang, L. M. Riedel, S. Seal and J. J. Hickman, *Biomaterials*, 2007, **28**, 1918–1925.
16 S. Deshpande, S. Patil, S. V. Kuchibhatla and S. Seal, *Appl. Phys. Lett.*, 2005, **87**, 133113.
17 C. Korsvik, S. Patil, S. Seal and W. T. Self, *Chem. Commun.*, 2007, 1056–1058.
18 I. Celardo, M. De Nicola, C. Mandoli, J. Z. Pedersen, E. Traversa and L. Ghibelli, *ACS Nano*, 2011, **5**, 4537–4549.
19 A. Filippi, F. Liu, J. Wilson, S. Lelieveld, K. Korschelt, T. Wang, Y. Wang, T. Reich, U. Pöschl, W. Tremel, H. Tong. RSC Adv. 2019, **9**, 11077–11081. (b) K. Reed, N. Bush, Z. Burns, G. Doherty, T. Foley, M. Milone, K. L. Maki, M. Cromer, Biomolecules 2019, **9**, 447.
20 (a) E. G. Heckert, A. S. Karakoti, S. Seal and W. T. Self, *Biomaterials*, 2008, **29**, 2705–2709. (b) Y. Xue, Y. Zhai, K. Zhou, L. Wang, H. Tan, Q. Luan and X. Yao, *Chem. Eur. J.*, 2012, **18**, 11115–11122.
21 S. Singh, T. Dosani, A. S. Karakoti, A. Kumar, S. Seal and W. T. Self, *Biomaterials*, 2011, **32**, 6745–6753.
22 R. Singh and S. Singh, *Colloids and Surfaces B: Biointerfaces*, 2015, **132**, 78–84.
23 K. J. Mitchell, K. A. Abboud and G. Christou, *Nature Commun.* 2017, **8**, 1445.
24 K. J. Mitchell, J. Goodsell, B. Russell-Webster, U. Twahir, A. Angerhofer, K. A. Abboud and G. Christou, *Inorg. Chem.*, 2021, **60**, 1641–1653.
25 B. Russell-Webster, J. Lopez-Nieto, K. A. Abboud and G. Christou, *Angew. Chem. Int. Ed. 2021,* **60**, 12591–12596
26 S. Babu, A. Velez, K. Wozniak, J. Szydlowska and S. Seal, *Chem. Phys. Lett.*, 2007, **442**, 405–408.
27 F. Menges, *Spectragryph - optical spectroscopy software*, 2020.
28 *Saint, Bruker-AXS: Madison, WI., USA, 2013.*, .
29 G. Sheldrick, *SHELXTL2014 (2014). Bruker-AXS, Madison, Wisconsin, USA.*, .
30 P. van der Sluis and A. L. Spek, *P. van der Sluis & A.L. Spek (1990). SQUEEZE, Acta Cryst. A46, 194-201*, 1990.
31 A. L. Spek, *Spek, A.L. (2009). PLATON, Acta Cryst. D65, 148-155*, .
32 V. Mereacre, A. M. Ako, M. N. Akhtar, A. Lindemann, C. E. Anson and A. K. Powell, *Helv. Chim. Acta,* 2009, **92**, 2507–2524.
33 J. Goura and V. Chandrasekhar, *Chem. Rev.*, 2015, **115**, 6854–6965.
34 C. Boskovic, M. Pink, J. C. Huffman, D. N. Hendrickson, G. Christou, *J. Am. Chem. Soc.* 2001, **123**, 9914-9915.
35 J. T. Brockman, K. A. Abboud, D. N. Hendrickson and G. Christou, *Polyhedron*, **2003**, *22*, 1765-1769.
36 B. Russell-Webster, K. A. Abboud and G. Christou, *Chem. Commun.*, 2020, **56**, 5382–5385.
37 C. Hennig, A. Ikeda-Ohno, W. Kraus, S. Weiss, P. Pattison, H. Emerich, P.M. Abdala and A. C. Scheinost, Inorg. Chem., 2013, 52(20), 11734–11743.

38 (G. Calvez, C. Daiguebonne, O. Guillou and F. Le Dret, *Eur. J. Inorg. Chem.*, 2009, **2009**, 3172–3178.
39 R. Das, R. Sarma and J. B. Baruah, *Inorg. Chem. Comm.*, 2010, **13**, 793–795.
40 S. L. Estes, M. R. Antonio and L. Soderholm, *J. Phys. Chem. C*, 2016, **120**, 5810–5818.
41 L. Mathey, M. Paul, C. Copéret, H. Tsurugi and K. Mashima, *Chem. Eur. J.*, 2015, **21**, 13454–13461.
42 T. C. Stamatatos, K. A. Abboud, W. Wernsdorfer and G. Christou, *Angew. Chem. Internat. Ed.*, 2006, **45**, 4134–4137.
43 E. E. Moushi, A. Masello, W. Wernsdorfer, V. Nastopoulos, G. Christou and A. J. Tasiopoulos, *Dalton Trans.*, 2010, **39**, 4978–4985.
44 M. Manoli, R. D. L. Johnstone, S. Parsons, M. Murrie, M. Affronte, M. Evangelisti and E. K. Brechin, *Angew. Chem. Internat. Ed.*, 2007, **46**, 4456–4460.
45 N. E. Brese and M. O'Keeffe, *Acta Cryst B*, 1991, **47**, 192–197.
46 I. D. Brown, *Chem. Rev.*, 2009, **109**, 6858–6919.
47 R. Si and M. Flytzani-Stephanopoulos, *Angew. Chem. Internat. Ed.*, 2008, **47**, 2884–2887.
48 Y. Xue, Q. Luan, D. Yang, X. Yao and K. Zhou, *J. Phys. Chem. C*, 2011, **115**, 4433–4438.
49 M. Lu, Y. Zhang, Y. Wang, M. Jiang and X. Yao, *ACS Appl. Mater. Interfaces*, 2016, **8**, 23580–23590.
50 Y. Zhai, K. Zhou, Y. Xue, F. Qin, L. Yang and X. Yao, *RSC Adv.*, 2013, **3**, 6833–6838.
51 T.-J. Whang, H.-Y. Huang, M.-T. Hsieh and J.-J. Chen, *Int J Mol Sci*, 2009, **10**, 4707–4718.
52 D. Heger, J. Jirkovsk and P. Kln, *J. Phys. Chem. A*, 2005, **109**, 6702–6709.
53 T. Fuenzalida and D. Fuentealba, *Photochem. Photobiol. Sci.*, 2015, **14**, 686–692.
54 K. Dutta, S. Mukhopadhyay, S. Bhattacharjee and B. Chaudhuri, *J. Hazardous Materials*, 2001, **84**, 57–71.
55 S. S. Lee, W. Song, M. Cho, H. L. Puppala, P. Nguyen, H. Zhu, L. Segatori and V. L. Colvin, *ACS Nano*, 2013, **7**, 9693–9703.
56 M. Spulber, P. Baumann, J. Liu and C. G. Palivan, *Nanoscale*, 2015, **7**, 1411–1423.